

TESTING THE PREDICTION OF FUZZY DARK MATTER THEORY IN THE MILKY WAY CENTER

ZHI LI ¹, JUNTAI SHEN ^{2,3,4,5}, AND HSI-YU SCHIVE ⁶

¹Tsung-Dao Lee Institute, Shanghai Jiao Tong University, Shanghai 200240, China; email: zli0804@sjtu.edu.cn

²Department of Astronomy, School of Physics and Astronomy, Shanghai Jiao Tong University, Shanghai 200240, China; email: jtshen@sjtu.edu.cn

³Shanghai Key Laboratory for Particle Physics and Cosmology, 200240, Shanghai, China

⁴Shanghai Astronomical Observatory, Chinese Academy of Sciences, 80 Nandan Road, Shanghai 200030, China

⁵College of Astronomy and Space Sciences, University of Chinese Academy of Sciences, 19A Yuquan Road, Beijing 100049, China

⁶Center for Theoretical Physics, National Taiwan University, Taipei 10617, Taiwan; email:hyschive@phys.ntu.edu.tw

ABSTRACT

The fuzzy dark matter model (FDM, also known as quantum wave dark matter model) argues that light bosons with a mass of $\sim 10^{-22}$ eV are a possible candidate for dark matter in the Universe. One of the most important predictions of FDM is the formation of a soliton core instead of a density cusp at the center of galaxies. If FDM is the correct theory of dark matter, then the predicted soliton core can help to form the Central Molecular Zone (CMZ) in the Milky Way. We present high-resolution hydrodynamical simulations of gas flow patterns to constrain the properties of the soliton core based on a realistic Milky Way potential. We find that a dense center is required to form a reasonable CMZ. The size and kinematics of the CMZ offer a relatively strong constraint on the inner enclosed mass profile of the Galaxy. If a soliton core is not considered, a compact nuclear bulge alone with a radially varying mass-to-light ratio can match the observed size and kinematics of the CMZ. A soliton core model with a mass of $\approx 4.0 \times 10^8 M_\odot$ and a core radius of ≈ 0.05 kpc, together with a less massive nuclear bulge with a constant mass-to-light ratio, also agrees nicely with the current data. Such a FDM soliton core corresponds to a boson mass of $\sim 2 - 7 \times 10^{-22}$ eV, which could be further constrained by the improved determination of the mass-to-light ratio in the Galactic center.

Keywords: galaxies: ISM — galaxies: kinematics and dynamics — galaxies: structures — galaxies: hydrodynamics — cosmology: dark matter

1. INTRODUCTION

Although the current cold dark matter (CDM) model successfully explains many problems on the large-scale structures of the universe (e.g. [Frenk & White 2012](#); [Bennett et al. 2013](#)), some of its predictions on the galactic scales are still in tension with modern observations (see the review by [Bullock & Boylan-Kolchin 2017](#)). One of the famous discrepancies is the so-called “cusp-core” problem: dissipationless CDM simulations predicted a universal Navarro-Frenk-White (NFW) density profile for bound dark matter halos, with a cuspy density profile at central part ([Navarro et al. 1997](#)); while observations favour a flat cored profile in low surface brightness galaxies (LSB) and dwarf galaxies ([de Blok 2010](#)). A shallower dark matter core might be created by considering the various baryonic effects in simulations (e.g. [Oñorbe et al. 2015](#); [Read et al. 2019](#)). However, it is still not clear how these “sub-grid physics” alter the structure formation in the lowest mass galaxies (e.g. [Sánchez et al. 2012](#); [Weinberg et al. 2015](#)).

On the other side, alternative dark matter models are being developed to solve the problems in a more self-consistent way. In recent years the Fuzzy Dark Matter model (FDM), also known as “quantum wave dark matter” model, is gaining more attention. In this scenario, the dark matter is composed of very light bosons with a particle mass of $\sim 10^{-22}$ eV (e.g. [Hu et al. 2000](#); [Marsh & Silk 2014](#); [Schive et al. 2014a](#)). Such bosons have a characteristic wavelength of $mv/\hbar \sim 0.2$ kpc assuming a velocity of 100 km s^{-1} , which helps to suppress the formation of small-scale structures. One of the most important predictions of FDM is the presence of a stable ground state soliton core due to the Bose-Einstein condensate at the central part of each dark matter halo. The core radius is usually comparable to the characteristic wavelength, and the halo transitions to a NFW profile within a few core radii according to recent numerical simulations (e.g. [Schive et al. 2014b](#)). This may provide a plausible solution to the “cusp-core” problem in CDM model. One can easily deduce that a lower mass

halo would host a larger soliton core due to the particles inside it having a smaller velocity and a larger characteristic wavelength. Therefore previous works (e.g. [Chen et al. 2017](#)) preferred to use dwarf galaxies to constrain the soliton core mass and size, and a boson mass of $1 - 2 \times 10^{-22}$ eV is favored in such studies.

Naturally, one may wonder whether the soliton core exists in our Milky Way and if so, how we can detect its effects on the stars and gas. The Milky Way should be a unique laboratory for testing the existence of such a soliton core due to the unprecedented data quality we could achieve compared to external galaxies. However, one should be careful when applying the halo-core scaling relation found in previous FDM simulations (e.g. [Schive et al. 2014b](#)) to the Milky-Way like galaxies to derive the soliton core properties. One reason is that previous FDM simulations focus mainly on the halo mass range of $10^9 - 10^{11} M_\odot$. It is not clear whether the scaling relation between the host halo mass and the central soliton core properties can be extrapolated to more massive halos, such as the Milky Way with a virial halo mass of $\approx 1.5 \times 10^{12} M_\odot$ ([Portail et al. 2017](#); [Li et al. 2019](#); [Posti & Helmi 2019](#)). Another reason is that the halo-core relation could be interpreted as the specific kinetic energy of the soliton core equals that of the halo. However, the specific kinetic energy of the soliton core can be strongly affected by the baryons in the Galactic center, and therefore the halo-core scaling relation may need to be adjusted. ([Bar et al. 2019](#), see also §2.1.3).

Nevertheless, according to the scaling relation in [Schive et al. \(2014b\)](#), the expected soliton mass and core radius are $1.44 \times 10^9 M_\odot$ and 0.16 kpc for the Milky Way, respectively, by assuming a boson mass of 1.0×10^{-22} eV. It is also important to note that these two numbers should be interpreted as the maximum soliton core mass and the minimum soliton core radius, due to the fact that the halo of the Milky Way may still be relaxing ([Hui et al. 2017](#)).

Observations on stellar and gas kinematics in the Galactic center have revealed some evidence for a central component with mass of $10^9 M_\odot$, although it is not clear whether this component is composed of baryons or dark matter (see the discussions in Sec.V.B of [Bar et al. 2018](#)). [Portail et al. \(2017\)](#) and [De Martino et al. \(2018\)](#) included such a component in their dynamical models to explain the high velocity dispersion of the stars in the Galactic bulge. Moreover, the Central Molecular Zone (CMZ, [Bally et al. 1988](#)) which is thought to be a molecular gas ring or disk orbiting the Galactic center, has a size of ≈ 100 pc (Galactic longitude $|l| \lesssim 1.5^\circ$) with a rotation velocity of ≈ 100 km s $^{-1}$ (e.g. [Molinari et al. 2011](#); [Kruijssen et al. 2015](#); [Henshaw et al. 2016](#)). This implies an enclosed mass of $\approx 2.3 \times 10^8 M_\odot$ inside ≈ 100 pc by assuming circular motions. The for-

mation of the CMZ is related to the bar-induced gas inflow due to the large-scale bi-symmetric gravitational torques (e.g. [Sormani et al. 2015a](#); [Li et al. 2016](#); [Ridley et al. 2017](#)). In addition, the CMZ needs a dense center ($\sim 1\%$ disk mass) to support its backbone x_2 orbits ([Regan & Teuben 2003](#); [Li et al. 2017](#); [Sormani et al. 2018a](#)). Previous studies usually included a very compact stellar nuclear bulge to form the CMZ (e.g. [Baba et al. 2010](#); [Li et al. 2016](#); [Shin et al. 2017](#); [Sormani et al. 2018a](#); [Armiglotta et al. 2019](#)), but the physical origin of this component is still not clear. The mass and size of the nuclear bulge are also not well-constrained, due both to dust extinction on the Galactic plane and to the uncertainties on the mass-to-light ratio of the nuclear bulge (see §2.1.2). This gives us some freedom to add a soliton core in our previous Milky Way gas dynamical model ([Li et al. 2016](#)) to see whether we could still reproduce the observed CMZ shape and kinematics, thus putting important constraints on the FDM theory.

The purpose of the present paper is to use high resolution hydrodynamical simulations to determine the allowed mass and size of the soliton core in the Milky Way. The paper is organized as follows: in §2 we describe our model setup and numerical methods; in §3 we present our simulation results; In §4 we discuss the possibility of the existence of such a soliton core together with its additional dynamical effects. The summary is presented in §5.

2. MODEL SETUP

2.1. Gravitational Potential

2.1.1. Realistic Milky Way Potential

The Galactic potential used in this work is based on the best-fit gas dynamical model of [Li et al. \(2016\)](#), where they used the features in (l, v) diagram to constrain the gas flow patterns in the Milky Way on large scales. The (l, v) diagram shows the intensity of cold gas emission as a function of Galactic longitude l and line-of-sight velocity v (e.g. [Dame et al. 2001](#)). The gaseous features viewed from face-on appear as high-density ridges in the (l, v) diagram, and these features are formed mainly due to the non-axisymmetric structures such as the Galactic stellar bar and spiral arms.

The large-scale potential of the Milky Way has been studied extensively in recent works. [Portail et al. \(2015\)](#) constructed a made-to-measure Milky Way model that matches the 3D density of red clump giants in the bulge region ([Wegg & Gerhard 2013](#)) and the BRAVA kinematics ([Kunder et al. 2012](#)) quite well. The axial ratios of the bar are (10:6.3:2.6) with the semi-major axis of ≈ 5 kpc. The bar angle to the Sun-Galactic center line is $(27 \pm 2^\circ)$. We adopt this model as the basis of the Galactic potential with a few minor modifications as in

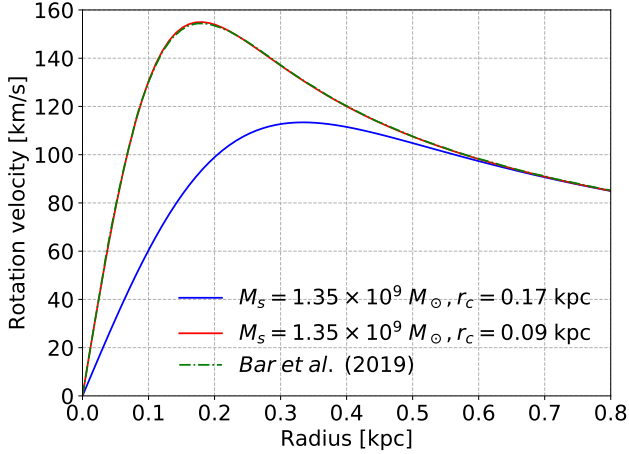


Figure 1. The rotation curves of a soliton core with a fixed mass of $1.35 \times 10^9 M_\odot$ but different core radius calculated by Eq. 3. In this plot we assume the virial mass of the Milky Way halo is $1.0 \times 10^{12} M_\odot$ and a boson particle mass of 1.0×10^{-22} eV, same as in Bar et al. (2019). The blue solid line shows the rotation curve of a self-gravitating soliton core with a core radius $r_c = 0.17$ kpc, while the red dotted-dash line shows a soliton core that is compressed by a factor of 2. The compressed soliton core has the same total mass but a smaller core radius $r_c = 0.09$ kpc. The green dotted-dashed curve shows the results from Bar et al. (2019) who obtained the compressed soliton core profile by directly solving Schrödinger-Poisson equation in an external nuclear bulge potential. Their results are in good agreement with Eq. 3.

Li et al. (2016). The bar pattern speed is chosen to be $\Omega_b = 33 \text{ km s}^{-1} \text{ kpc}^{-1}$, which places the corotation radius at $R = 6.2$ kpc. In this study we remove the large-scale spiral potentials from Li et al. (2016) as they are only important for the outer gas features, which is not the main focus of this work.

On the other hand, the central mass distribution in our Galaxy is not well-constrained. The stellar kinematics may only be reliable at higher latitudes ($b \geq 2^\circ$), due to the heavy dust contamination closer to the disk plane. The gas kinematics in the central disk region may not serve as a good indicator of mass either, due to its highly non-circular motions caused by the Galactic bar (e.g. Fux 1999; Sormani et al. 2015b, 2018b). We therefore modify the central potential of the best-fit model in Li et al. (2016) to test the possible effects caused by a soliton core. We include the following two components, namely the nuclear bulge and the soliton core, in the central part of the Milky Way potential.

2.1.2. Nuclear bulge

Launhardt et al. (2002) found hints of a stellar nuclear bulge component in the central ~ 200 pc of the Milky Way using COBE near-infrared image. The authors parameterized the nuclear bulge with the following

equation:

$$\rho_{\text{nb}}(R, z) = 32.4 \Upsilon \exp \left\{ -0.693 \left[\left(\frac{R}{R_{\text{nb}}} \right)^5 + \left(\frac{z}{0.045 \text{ kpc}} \right)^{1.4} \right] \right\} M_\odot \text{ pc}^{-3}, \quad (1)$$

where Υ is the mass-to-light ratio, and R_{nb} is the scale radius of the nuclear bulge. Launhardt et al. (2002) used two components with different scale radii, $R_{\text{nb},1} = 120$ pc and $R_{\text{nb},2} = 220$ pc, to fit the data. The authors claimed that the presence of two distinct components may not have a clear physical meaning, but could reflect the extinction effects not accounted for in their model. By assuming $\Upsilon = 2$, Launhardt et al. (2002) derived the total mass of the nuclear bulge to be $(1.4 \pm 0.6) \times 10^9 M_\odot$.

Following Launhardt et al. (2002), the nuclear bulge included in our simulations is also composed of two components with $R_{\text{nb},1} = 120$ pc and $R_{\text{nb},2} = 220$ pc. Their density profiles are described by Eq. 1. We generally assume the mass-to-light ratio Υ is the same for the two components. The total mass of the nuclear bulge is therefore $1.4 \times 10^9 M_\odot$ with $\Upsilon_1 = \Upsilon_2 = 2.0$, consistent with Launhardt et al. (2002). In Section 3.2 we test a slightly different nuclear bulge mass model where $\Upsilon_1 = 3.46$ and $\Upsilon_2 = 0$.

As the nuclear bulge is a massive and compact object, its dynamical effects cannot be negligible. Other studies have also revealed the presence of the nuclear bulge (or at least a massive and dense central object), including the young stellar nuclear disk found in APOGEE by Schönrich et al. (2015), and the increase of stellar velocity dispersion caused by a massive central object in Portail et al. (2017) and De Martino et al. (2018). Li et al. (2016) also included the nuclear bulge to generate a reasonable CMZ in their best-fit gas dynamical models. However, the exact mass of the nuclear bulge is still not well determined. This is partly because that the COBE photometry used to derive the density profile of the nuclear bulge is heavily affected by the dust extinction. Another reason is that the assumed $\Upsilon = 2$ in the near-infrared band is uncomfortably large (e.g. Conroy et al. 2009; Conroy & Gunn 2010). We therefore keep Υ as a free parameter in this study.

2.1.3. Soliton core

FDM simulations found a tight relation between the central soliton core properties and the host halo mass (Schive et al. 2014b), although this relation may not be very accurate to predict the soliton core properties in the Milky Way, as noted in the introduction. The virial mass of the Milky Way halo has been constrained to be around $0.9 - 2.0 \times 10^{12} M_\odot$ (e.g. Portail et al. 2017; Posti & Helmi 2019). Applying the halo-core relation in Schive

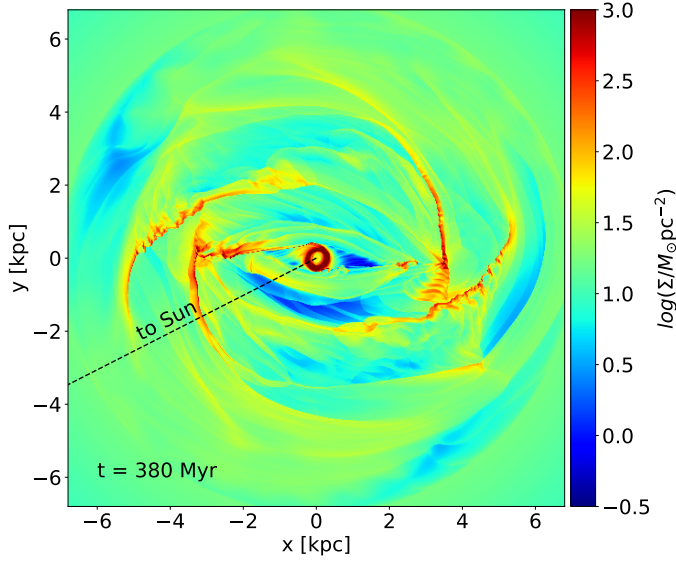


Figure 2. The gas surface density Σ in our hydrodynamical simulations with $c_s = 10 \text{ km s}^{-1}$. The bar lies horizontally along x -axis with a semi-major length around $\approx 5 \text{ kpc}$, and the corotation radius of the bar is placed at $R = 6.2 \text{ kpc}$. The CMZ can be seen as the high density gas ring around $R \approx 300 \text{ pc}$. The central potential in this model includes a nuclear bulge with $\Upsilon = 2$ but without a soliton core. The Sun is at $(x, y) = (-7.4 \text{ kpc}, -3.8 \text{ kpc})$ in this plot. The Sun-Galactic center line ($l = 0$) is indicated by the black dashed line.

et al. (2014b) with $m_{22} = 1$ and $M_{\text{halo}} = 1.5 \times 10^{12} M_{\odot}$, the expected soliton mass M_s and core radius r_c in the Milky Way are $M_s = 1.44 \times 10^9 M_{\odot}$ and $r_c = 0.16 \text{ kpc}$, respectively. Here m_{22} is the boson particle mass in unit of $1.0 \times 10^{-22} \text{ eV}$, and r_c is the core radius defined as the radius enclosing 25% of the total soliton mass M_s (r_c is also roughly the radius where density decreases to half of the central peak value). However, as pointed out in Section II.C from Hui et al. (2017), these two numbers should be interpreted only as the upper and lower limits, i.e. the maximum soliton mass and the minimum soliton core radius since the Milky Way halo may have not been fully relaxed and the soliton core may be developing. We therefore define $M_{\text{smax}} = 1.44 \times 10^9 M_{\odot}$ as the maximum soliton mass inside the Milky Way by adopting $m_{22} = 1$. Note that this mass is very close to the mass of the nuclear bulge with $\Upsilon = 2$.

The mass M_s and core radius r_c of self-gravitating soliton cores are inversely related, since the characteristic de Broglie wavelength cannot exceed the virial radius of the system (Hui et al. 2017, also see Eq. 5 in §3.5). This relation needs to be modified for the Milky Way, due to the presence of the nuclear bulge whose mass and size are similar to the expected soliton core predicted by the halo-core relation. Recently, Bar et al. (2019) studied how the baryonic nuclear bulge would affect the soliton core size in the Milky Way. They found that the soli-

ton core radius r_c could be compressed to be half of its original value in the potential of a nuclear bulge with a mass profile similar to Launhardt et al. (2002). Inspired by their work, we adopt a modified soliton core density profile based on the results in Schive et al. (2014b) as:

$$\rho_{\text{soliton}}(r) = \frac{0.082 (r_c/\text{kpc})^{-3} (M_s/10^9 M_{\odot})}{[1 + 9.1 \times 10^{-2} (r/r_c)^2]^8} M_{\odot} \text{ pc}^{-3}, \quad (2)$$

where M_s and r_c are independent. We could then use Eq. 2 to make soliton cores with the same mass but different core radius. The corresponding gravitational acceleration of such a soliton core is given by:

$$a_{\text{soliton}}(r) = 1.82 \times 10^{-4} G M_s \frac{1}{r^2(b^2 + 1)^7} (3465b^{13} + 23100b^{11} + 65373b^9 + 101376b^7 + 92323b^5 + 48580b^3 - 3465b + 3465(b^2 + 1)^7 \arctan(b)), \quad (3)$$

where $b = (2^{1/8} - 1)^{1/2}(r/r_c)$ and $G = 4.302 \text{ kpc (km s}^{-1})^2 (10^6 M_{\odot})^{-1}$.

Assuming M_s and r_c are independent implies the mass profile of the nuclear bulge varies accordingly. This parametrisation is more flexible to obtain the required mass profile of the soliton core, while the method in Bar et al. (2019) is a more self-consistent way to determine the soliton core properties by solving the Schrödinger-Poisson equation. In this study, we first adopt M_s and r_c as two free soliton parameters. We then examine whether the preferred soliton core properties (i.e. certain combinations of M_s and r_c) are allowed by the nuclear bulge potential we adopt in §3.5.

If M_s and r_c are chosen to be the same as the predictions of the halo-core relation (Schive et al. 2014b), one gets a self-gravitating soliton core. If M_s is the same but a smaller r_c is adopted, one gets a compressed soliton core under an external baryonic potential (i.e. the nuclear bulge). In Fig. 1 we show the rotation curves obtained by Eq. 3 of a self-gravitating soliton core and a compressed soliton core with the same total mass. Our result is very similar to Fig. 4 in Bar et al. (2019). Note that $M_s = M_{\text{smax}} = 1.44 \times 10^9 M_{\odot}$ and $r_c = 0.16 \text{ kpc}$ correspond to the original halo-core relation predictions for a $M_{\text{halo}} = 1.5 \times 10^{12} M_{\odot}$ Milky Way mass halo and $m_{22} = 1$ (Schive et al. 2014b).

2.2. Numerical Scheme

We study how a thin gas disk evolves under a realistic barred Milky Way potential described in the previous sections. The barred potential is rigidly rotating about the Galactic center with a fixed pattern speed $\Omega_b = 33 \text{ km s}^{-1} \text{ kpc}^{-1}$. The gas is assumed to be inviscid, and we use the latest public version of the grid-based MHD code *Athena++* (Stone et al. in preparation) to solve the Euler equations. *Athena++* is a

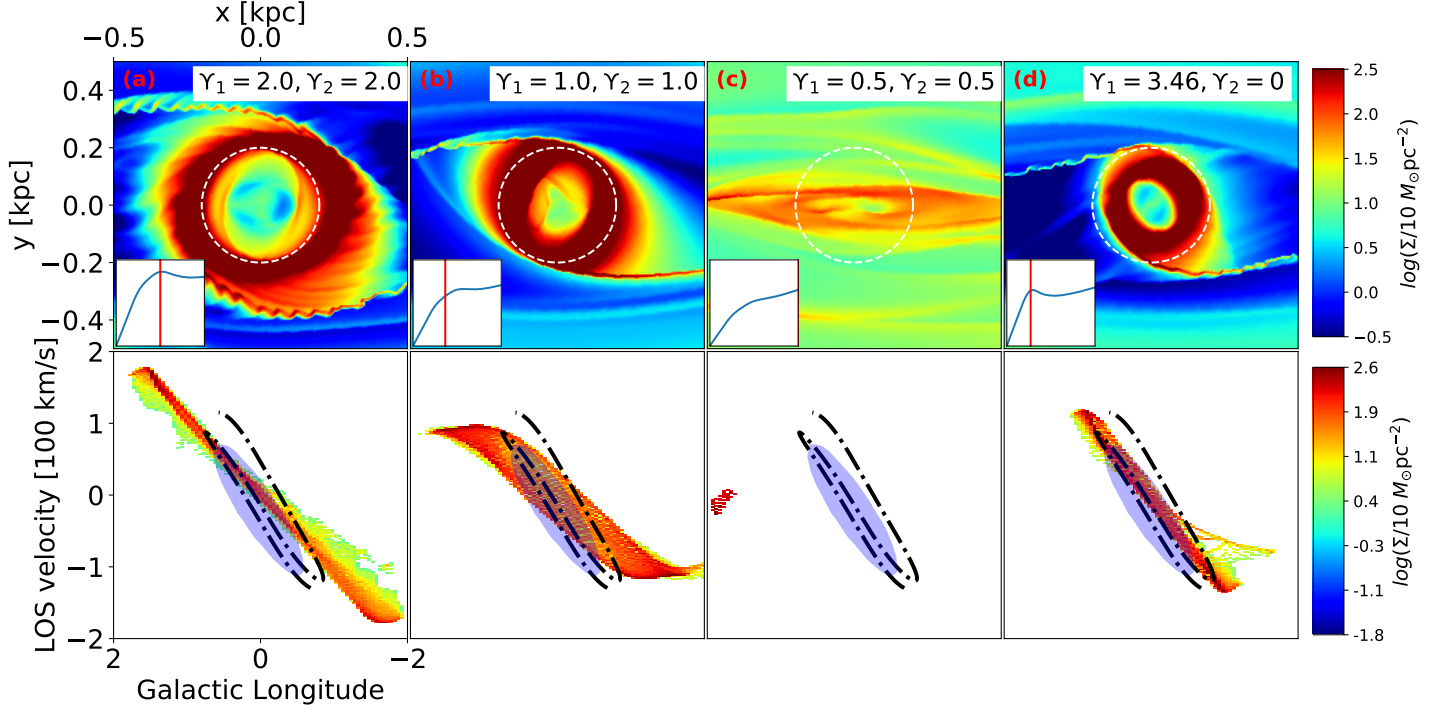


Figure 3. Effects of the mass-to-light ratio Υ of the nuclear bulge on the shape and kinematics of the CMZ, with a sound speed $c_s = 10 \text{ km s}^{-1}$. No soliton cores have been included in these four models. The snapshots are taken at $T = 500 \text{ Myr}$. Top panels: gas surface density in the inner 500 pc. From left to right Υ is decreased from 2 to 0.5, corresponding to a mass from $1.4 \times 10^9 M_\odot$ to $3.5 \times 10^8 M_\odot$. The white dashed circle denotes a radius of 200 pc, representing the outer boundary of the CMZ. The inset at the bottom left corner shows the rotation curve (blue line) and the averaged ring radius (vertical red line) in the model. The boundary of the inset is 500 pc for x -axis and 200 km s^{-1} for y -axis. The inset in panel (c) does not show a ring radius since the density of gas is not high enough to be called a CMZ (criteria: $\Sigma \geq 2 \times 10^3 M_\odot \text{ pc}^{-2}$). Bottom: (l, v) diagrams of the models, which show the distribution of gas density as a function of Galactic longitude l and line-of-sight velocity v . The limits of the colorbar are chosen to highlight most of the features in (l, v) space. The black dotted-dashed line is the open stream model of the CMZ proposed by Kruijssen et al. (2015). The blue shaded region shows the $[\text{CII}]$ observations in CMZ from Langer et al. (2017). The bottom part of panel (c) is almost empty because there are few dense gas in this model that satisfies our CMZ criteria. Note that Galactic longitude of 2° corresponds to a radius of $\approx 300 \text{ pc}$.

complete re-write of the previous *Athena* code with improved performance and scalability. We employ a uniform Cartesian grid with 4096×4096 cells for 2D simulations covering a square box with size of $L = 14 \text{ kpc}$, thus the grid spacing is $\Delta x = \Delta y = 3.4 \text{ pc}$. We also test 3D runs where the grid is $2048 \times 2048 \times 21$ with a vertical extent of 200 pc. We adopt the *roe* Riemann solver, piece-wise linear reconstructions, and outflow boundary conditions at the domain boundaries. High spatial resolution is necessary to capture the turbulent gas motions in the central region of galaxies, as demonstrated in previous works (e.g. Sormani et al. 2015a; Li et al. 2015; Few et al. 2016). All our models are run for a period of 0.5 Gyr. The 2D simulations take about $\sim 15\text{--}20$ hours using 64 INTEL cores, and the 3D runs take about ~ 5 days using 256 INTEL cores. In general, *Athena++* is ~ 5 times faster than the previous version *Athena* (Gardiner & Stone 2005; Stone et al. 2008; Stone & Gardiner 2009).

We set up the initial rotating gaseous disk

with an exponential surface density profile $\Sigma_{\text{gas}} = \Sigma_0 \exp(-R/R_d)$, where $\Sigma_0 = 76.7 M_\odot \text{ pc}^{-2}$ and $R_d = 4.8 \text{ kpc}$. The gas disk then has a surface density around $13 M_\odot \text{ pc}^{-2}$ at solar neighbourhood to match the observed value roughly (Bovy & Rix 2013). The initial rotation velocity of gas is set to balance the azimuthally averaged gravitational force. We linearly ramp up the bisymmetric bar potential over the first bar rotation period $T_{\text{bar}} = 186 \text{ Myr}$ to avoid transients. We compute the gas flow in the inertial frame, while Li et al. (2016) computed it in the bar corotation frame.

We adopt an isothermal equation of state assuming the specific gas internal energy is constant by an energy balance between radiative heating and cooling processes, same as previous studies (e.g. Kim et al. 2012b,a; Sormani et al. 2015c). The effective isothermal sound speed c_s describes the level of velocity dispersion between molecular clouds, thus does not stand for the microscopic gas temperature. We test two different c_s in our models with low (10 km s^{-1}) and high (20 km s^{-1})

cases, in the range of the observed ISM velocity dispersion (e.g. [Walter et al. 2008](#); [Leroy et al. 2009](#)). We neglect gas self-gravity, magnetic fields, star formation and stellar feedback, and other additional physics in our models for simplicity, but prefer to study these effects in a follow-up paper. We discuss how these unaccounted physics will affect our results in §4.4.

3. SIMULATION RESULTS

3.1. General evolution

We first report the simulation of the gas evolution in the potential described in §2.1 with a $\Upsilon = 2$ nuclear bulge, but without a soliton core. We explore the case with a relatively low sound speed $c_s = 10 \text{ km s}^{-1}$, which is the same as most of the previous studies (e.g. [Fux 1999](#); [Rodriguez-Fernandez & Combes 2008](#); [Ridley et al. 2017](#)). In Fig. 2 we show the gas surface density in the simulation at $t = 380 \text{ Myr}$ when the bar has finished about two rotation period. Strong shocks develop at the leading side of the bar as the flow is supersonic, which are indicated by the high density gas ridges in Fig. 2. Gas loses energy and angular momentum when encountering the shocks, then flows inwards and accumulates at center. The CMZ can be clearly seen as the high density ring-like structure at $R \approx 300 \text{ pc}$ in the center. The four spiral arms around the bar region are known as the near and far 3-kpc arms and the molecular ring in the (l, v) diagram, which are related to the 4:1 resonance of the rotating bar ([Sormani et al. 2015b](#)). The flow pattern then becomes quasi-steady until the end of the simulation.

In general, this model is very similar to the best-fit model of [Li et al. \(2016\)](#), as we adopt the same Galactic potential but with a higher resolution. In the following sections we vary the mass-to-light ratio Υ of the nuclear bulge, the mass of the soliton core M_s , and the radius of the soliton core r_c to determine the possible mass and size of the soliton core allowed in the Milky Way, thus putting constraints on FDM theory.

3.2. Tests with only the nuclear bulge

As we have shown in §2.1.2, An assumed a mass-to-light ratio $\Upsilon = 2$ gives a nuclear bulge mass of $1.4 \times 10^9 M_\odot$, which is very close to the maximum mass of the soliton core $M_{\text{smax}} = 1.44 \times 10^9 M_\odot$ with $m_{22} = 1$. However, the total mass of the central components is constrained to be $\approx 1.5 \times 10^9 M_\odot$ (e.g. [Launhardt et al. 2002](#); [Portail et al. 2017](#); [De Martino et al. 2018](#)). It is therefore not reasonable that the Milky Way hosts both a maximum mass soliton core and a $\Upsilon = 2$ nuclear bulge at the same time. The mass degeneracy of a soliton core and a stellar nuclear bulge in the Milky Way center was also discussed in [Bar et al. \(2018\)](#). As Υ of the nuclear bulge may have some uncertainties, we first examine its

effects on gas features when a possible soliton core is not included.

In Fig. 3 we plot the gas surface density (top panels), the rotation curves in the central 500 pc with the position of the CMZ marked (insets), and the corresponding (l, v) diagram (bottom panels) of the gas in the central 500 pc of our simulations with different Υ . The colors in the (l, v) diagram indicate gas density which is binned according to Galactic longitude and line-of-sight velocity. We only select the dense gas ($\Sigma \geq 2 \times 10^3 M_\odot \text{ pc}^{-2}$) to represent the CMZ and show their corresponding (l, v) features, therefore the colors in (l, v) diagrams are mostly red. The blue shaded region in the bottom panels indicates $[\text{CII}]$ observations in the CMZ region from [Langer et al. \(2017\)](#), while the dotted-dashed line is the open stream model of the CMZ obtained by fitting the NH_3 data ([Kruijssen et al. 2015](#)). The $[\text{CII}]$ mainly traces the hot ionized gas, while NH_3 originates from cold and dense molecular gas. It seems that gas with different physical conditions in the CMZ forms a consistent shape in the (l, v) space.

To form a CMZ that has similar size and kinematics compared to observations, the model needs to satisfy (at least) two conditions: (1) the rotation curve in the model has a circular velocity of $\approx 100 \text{ km s}^{-1}$ at $R \approx 100 \text{ pc}$; (2) the inflowed gas piles up on roughly circular orbits with $R \approx 100 \text{ pc}$. In Fig. 3 we show that the size of the CMZ shrinks with lower Υ , due to a decreasing central mass (e.g. [Athanasoulas 1992](#); [Regan & Teuben 2003](#); [Li et al. 2015, 2017](#)). For $\Upsilon = 0.5$, a central mass of $3.6 \times 10^8 M_\odot$ is not sufficiently massive to produce a nearly-circular CMZ with high gas density. The model with $\Upsilon = 2$ roughly satisfies condition (1), but the radius of CMZ is larger than the preferred value. The white dashed circle in the plot has a radius of 200 pc, which indicates the outer boundary of the CMZ (e.g. [Molinari et al. 2011](#); [Sormani & Barnes 2019](#)). On the other hand, the model with $\Upsilon = 1$ roughly satisfies condition (2), but the rotation velocity is lower, and thus it forms a shallower slope in the (l, v) diagram compared to observations. These results imply that varying Υ of the nuclear bulge alone with the density profile given by Eq. 1 may not produce a reasonable CMZ that is consistent with observations in both size and kinematics.

We slightly fine-tune the model of the nuclear bulge above to see whether we could better reproduce the observed CMZ kinematics. We find a less massive but more concentrated nuclear bulge is needed to satisfy conditions (1) and (2) simultaneously. Fig. 3(d) shows such a model with $\Upsilon_1 = 3.46$ for the first component ($R_{\text{nb},1} = 120 \text{ pc}$), and $\Upsilon_2 = 0$ for the second component ($R_{\text{nb},2} = 220 \text{ pc}$). This results in a nuclear bulge with a mass of $5.1 \times 10^8 M_\odot$. The gas kinematics in Fig. 3(d) agree with observations fairly well. We re-

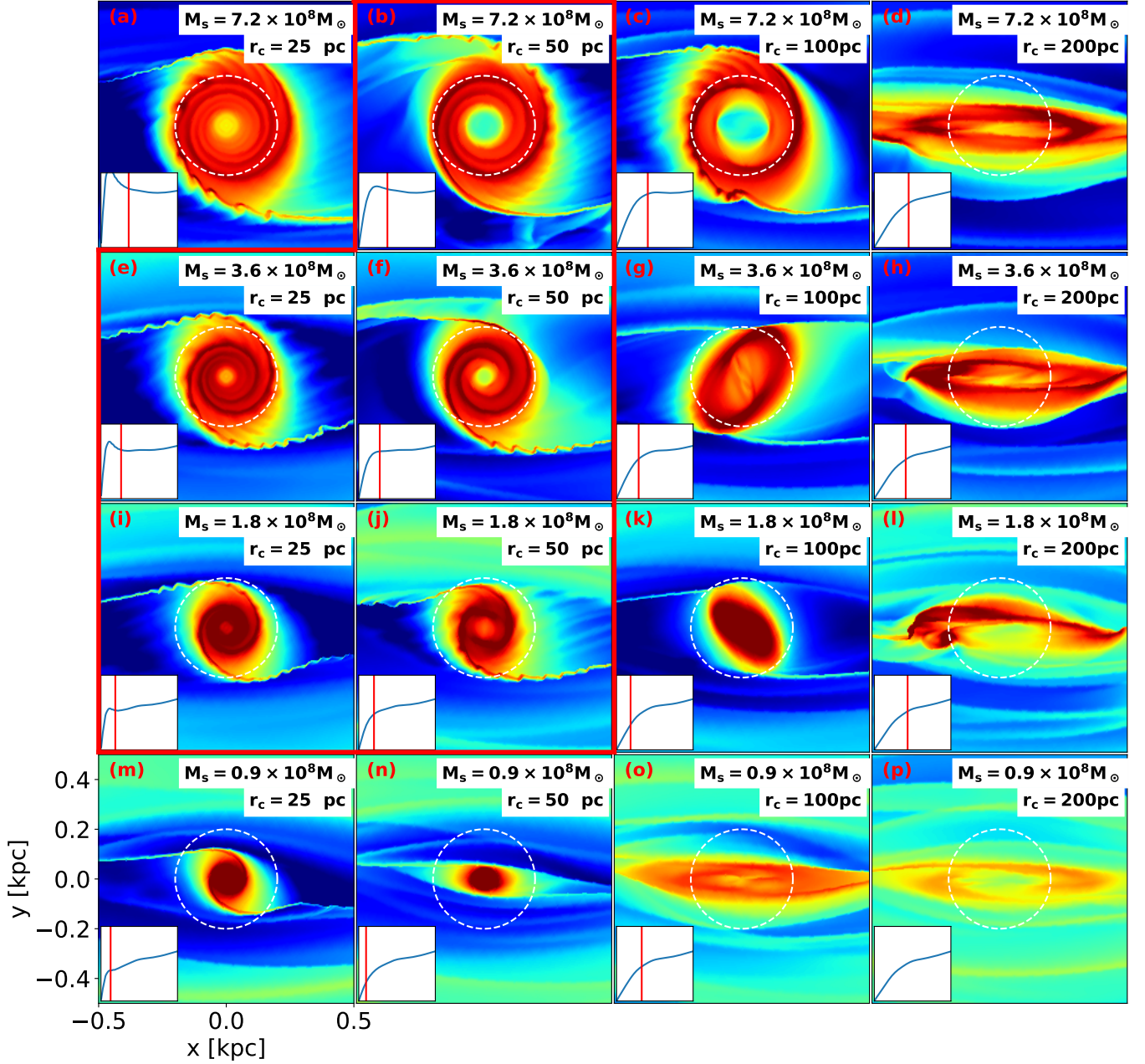


Figure 4. Gas surface density in the inner 500 pc for the models that include a nuclear bulge with $\Upsilon = 0.5$ and a soliton core with different mass and size. The lines, symbols, and the color map are identical to those in Fig. 3. The snapshots are taken at $T = 500$ Myr. From left to right the soliton core radius r_c increases from 25 pc to 200 pc, and from top to bottom the mass of the soliton core M_s decreases from $7.2 \times 10^8 M_\odot$ ($1/2 M_{\text{smax}}$) to $0.9 \times 10^8 M_\odot$ ($1/16 M_{\text{smax}}$). $M_{\text{smax}} = 1.44 \times 10^9 M_\odot$ is the maximum soliton mass inside a $1.5 \times 10^{12} M_\odot$ Milky Way halo predicted by the halo-core relation in [Schive et al. \(2014b\)](#) assuming $m_{22} = 1$. Note that M_{smax} is very close to the mass of the nuclear bulge derived in [Launhardt et al. \(2002\)](#). The sound speed c_s is 10 km s^{-1} . The inset in the bottom right panel does not have a ring radius since the density of gas is not high enough, similar to Fig. 3. The red box highlights the models that roughly match the observed CMZ size.

gard this model which does not include a soliton core as one of our best-fit models, although the nuclear bulge density profile in this model is slightly different from that in [Launhardt et al. \(2002\)](#). If the luminosity profile in [Launhardt et al. \(2002\)](#) is correct, then this best-fit model implies that the mass-to-light ratio of the nuclear

bulge is radially varying.

3.3. Tests with possible soliton cores

In §2.1.3 we argue that the soliton core (if it exists) could be significantly compressed by the presence of a nuclear bulge. The compressed soliton core would result in a steeper rotation curve at the inner region, which

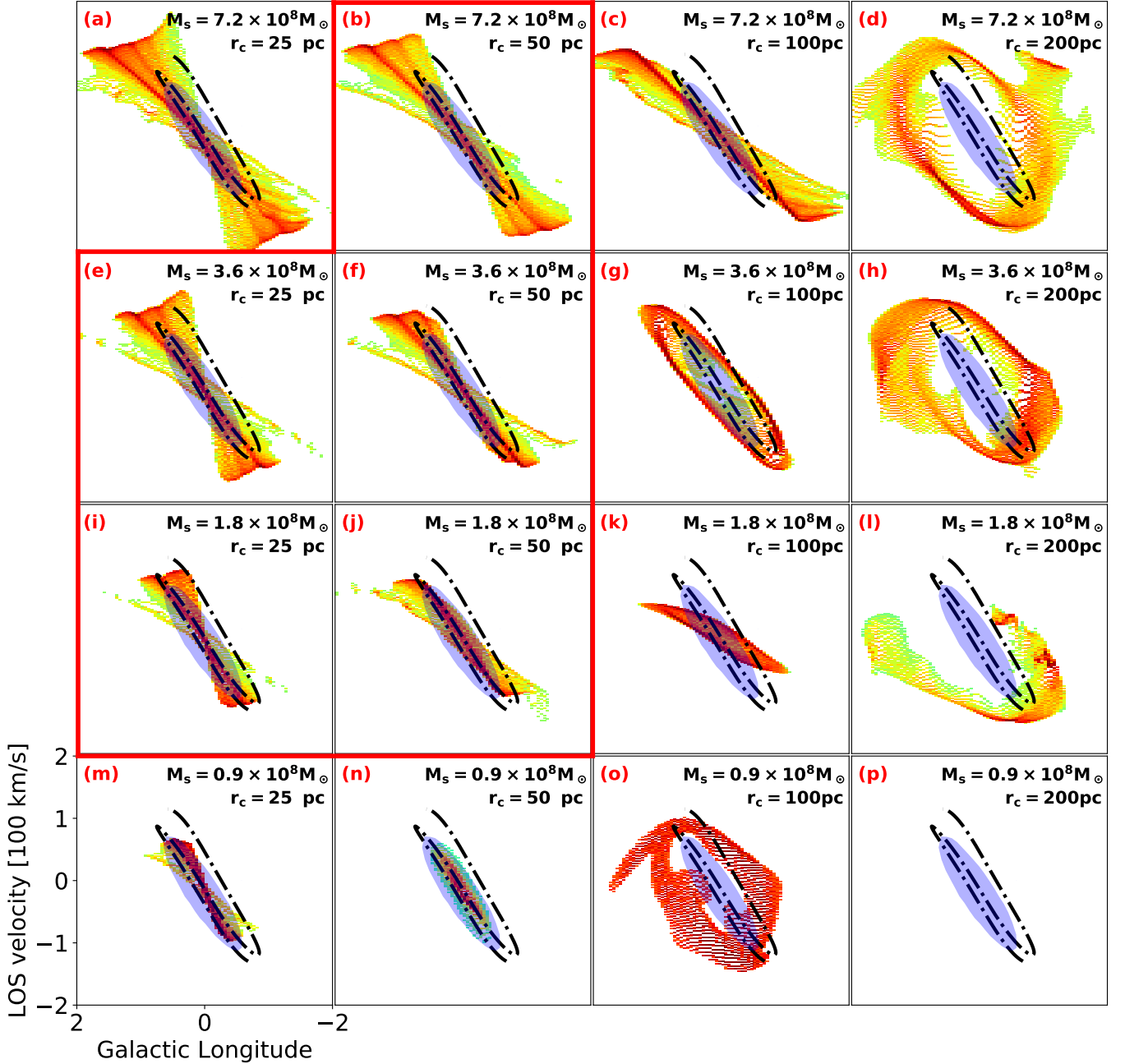


Figure 5. The (l, v) diagram in the inner 2° of Galactic longitude l for the models shown in Fig. 4. The lines, symbols, and the color map are identical to those in Fig. 3. The bottom right panel is almost empty because the density of gas is not high enough in this model, similar to Fig. 3. The red box highlights the models that can roughly reproduce the observed CMZ kinematics.

helps to generate a steeper slope in the (l, v) space for the CMZ. In the following sections we adopt the nuclear bulge profile as determined in [Launhardt et al. \(2002\)](#), where the mass-to-light ratio is the same for the two components. As shown in §3.2, such a nuclear bulge is not concentrated enough, thus leaves some room for a compressed soliton core.

Fig. 3(b) suggests a $\Upsilon = 1$ nuclear bulge already generates a slightly larger CMZ compared to observations. Adding a compact soliton core together with such a nu-

clear bulge would only make the CMZ even larger. We thus adopt $\Upsilon = 0.5$ for the nuclear bulge so that we can produce a CMZ smaller than 200 pc by including a suitable soliton core.

Fig. 4 and Fig. 5 present the gas surface density and the corresponding (l, v) diagram for the models with different soliton core mass M_s and core radius r_c , together with a $\Upsilon = 0.5$ nuclear bulge. From left to right the core radius r_c are 25 pc, 50 kpc, 100 pc and 200 pc, respectively. From top to bottom the soliton

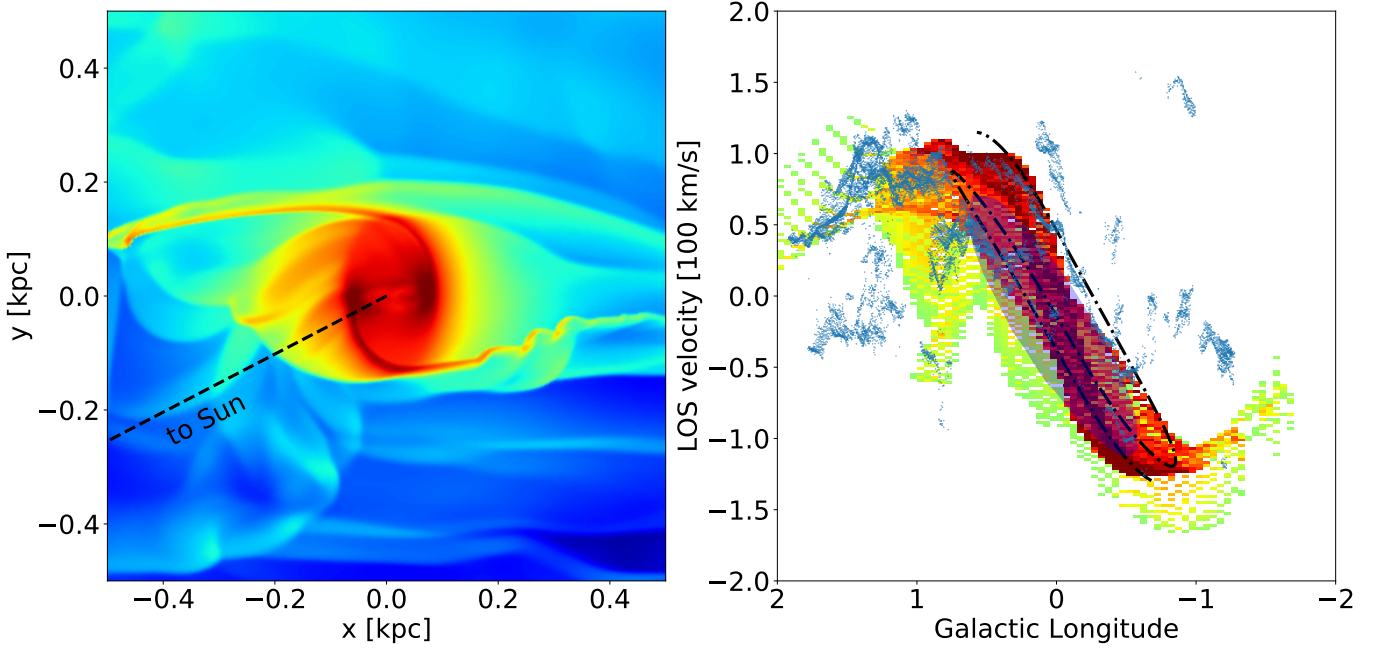


Figure 6. Gas surface density and the corresponding (l, v) diagram with $c_s = 20 \text{ km s}^{-1}$. The lines, symbols, and the color map are identical to those in Fig. 3. The model includes a nuclear bulge with $\Upsilon = 0.5$ and a soliton core of $M_s = 3.6 \times 10^8 M_\odot$ and $r_c = 50 \text{ pc}$. This model is almost identical to panel (f) in Fig. 4 and 5, except that the sound speed is twice higher. The blue dots in the right panel are NH_3 data from HOPS survey (Longmore et al. 2017) fitted by the SCOUSE package (Henshaw et al. 2016). The snapshot is taken at $T = 500 \text{ Myr}$. The (l, v) diagram of this model resembles most of the observed features.

core mass M_s are $7.2 \times 10^8 M_\odot$ ($1/2 M_{\text{smax}}$), $3.6 \times 10^8 M_\odot$ ($1/4 M_{\text{smax}}$), $1.8 \times 10^8 M_\odot$ ($1/8 M_{\text{smax}}$), and $0.9 \times 10^8 M_\odot$ ($1/16 M_{\text{smax}}$). $M_{\text{smax}} = 1.44 \times 10^9 M_\odot$ is the maximum soliton mass inside a $1.5 \times 10^{12} M_\odot$ Milky Way halo predicted by the halo-core relation in Schive et al. (2014b) assuming $m_{22} = 1$. The blue line at the inset of each panel denotes the rotation curve, and the vertical red line is the averaged CMZ radius, same as in Fig. 3.

It is clear that the location of CMZ is roughly the the turnover radius of the rotation curve (i.e. where the rotation curve turns flat). For the detailed formation mechanism we refer the reader to Li et al. (2015). The effects of different soliton core mass M_s and core radius r_c are similar to those of varying Υ of the nuclear bulge. A larger M_s leads to a larger CMZ, while a smaller r_c produces a more circular CMZ together with a steeper (l, v) feature. Combining Figs. 4 and 5, we conclude that cases (b), (e), (f), (i) and (j) can roughly satisfy conditions (1) and (2) mentioned in §3.2 simultaneously. The CMZ formed in these five simulations better reproduce the observed gas kinematics together with a size of $\approx 200 \text{ pc}$. These five models are highlighted with a red box in the figures, and are regarded as our best-fit models that contain a soliton core.

The soliton cores with larger r_c form more elliptical CMZs compared to models with smaller r_c . The orientation of these more elliptical CMZs oscillates with time, which is not shown here but can be inferred in panel (g)

and (k) in Fig. 4. This is because that gas tend not to follow periodic orbits when the pressure force is comparable to the gravitational force. The oscillating CMZ is more or less similar to the open stream model proposed by Kruijssen et al. (2015), who argued that a processing orbit instead of a closed orbit is a more physical solution in a Galactic potential. In our models, when these elliptical CMZs have a specific angle with respect to the Sun, the resulting (l, v) plot agrees better with observations (e.g. panel g), while other angles are worse (e.g. panel k). This can be understood by the following arguments: The Sun is at $(x, y) = (-7.4 \text{ kpc}, -3.8 \text{ kpc})$ in our models (also see the dashed Sun-Galactic center line in Fig. 6), if the line-of-sight is tangent to the elliptical CMZ near its pericenter (e.g. panel g), we would expect a steeper slope in the (l, v) space due to a higher LOS velocity and a narrower extent compared to the case where the tangent point is near the apocenter (e.g. panel k). It is possible that the shape of the CMZ changes with time in reality, but it then implies we are observing the CMZ at a special time. If this is true, the constraints on the soliton core radius r_c could be loosened to a slightly larger value.

3.4. Varying sound speed

Apart from the gravitational constraints, the gas in the CMZ is also quite turbulent. ALMA observations of SiO revealed the velocity dispersion of gas can be as

large as $\sim 20 \text{ km s}^{-1}$ (Kauffmann 2016). The NH_3 data from HOPS survey (Longmore et al. 2017) indicate a velocity dispersion of $17.4 \pm 4.8 \text{ km s}^{-1}$. As described in §2.2, the effective isothermal sound speed c_s used in our simulations reflects mainly the velocity dispersion of gas clouds. We therefore further test a higher value $c_s = 20 \text{ km s}^{-1}$ for the preferred models highlighted by the red box in Fig. 5 to see how this would affect our results.

We find that a higher sound speed c_s generally makes the CMZ smaller, but only slightly. This is because shocks with a higher c_s are developed closer to the bar major axis. The physical reason is that the gas is less supersonic thus needs a steeper potential to be shocked (e.g. Kim et al. 2012b; Sormani et al. 2015a). We also find that the CMZ tends to be more elliptical in a higher c_s case, similar to the model with a large core radius r_c but a lower c_s . A higher c_s also helps to broaden the (l, v) features as a result of a higher velocity dispersion, which better matches the data. Fig. 6 shows the model that matches most observed (l, v) features. The model hosts a nuclear bulge with $\Upsilon = 0.5$, together with a soliton core of $M_s = 3.6 \times 10^8 M_\odot$ and $r_c = 50 \text{ pc}$. This model is almost identical to panel (f) in Fig. 4 and 5, except with a $c_s = 20 \text{ km s}^{-1}$ instead of 10 km s^{-1} . The dashed line in the left panel indicates the Sun-Galactic center line (i.e. $l = 0^\circ$). The blue dots on the right panel show the NH_3 observations in the CMZ from HOPS survey (Longmore et al. 2017) fitted by the SCOUSE package (Henshaw et al. 2016).

It is interesting that the model shown in Fig. 6 also qualitatively reproduces the asymmetry of the CMZ, i.e. it shows more emission on the positive longitude compared to the negative longitude in the (l, v) space. From the face-on view, we can see that the gas forms some feather-like features on the left side of the CMZ. This may be caused by the “wiggling” instability proposed by Wada & Koda (2004) then further studied by Kim et al. (2014) and Sormani et al. (2017). A higher c_s enhances the instability, thus making the asymmetry more prominent than the lower c_s case. Some of the “feathers” roughly reproduces the observed Sagittarius B2 cloud at $l \approx 1^\circ$. It is worth noting that the asymmetry is transient, with a typical timescale of a few tens Myr, similar to some of the more sophisticated simulations (e.g. Sormani et al. 2018b).

We thus conclude that a model with a light and compact soliton core (i.e. $M_s \approx 3.6 \times 10^8 M_\odot$ and $r_c \approx 50 \text{ pc}$), together with a $\Upsilon = 0.5$ nuclear bulge can roughly reproduce most of the observed CMZ properties. The match is better when adopting a higher sound speed $c_s \approx 20 \text{ km s}^{-1}$. Nevertheless, it is still worth exploring for a better match to the observed features in the future studies.

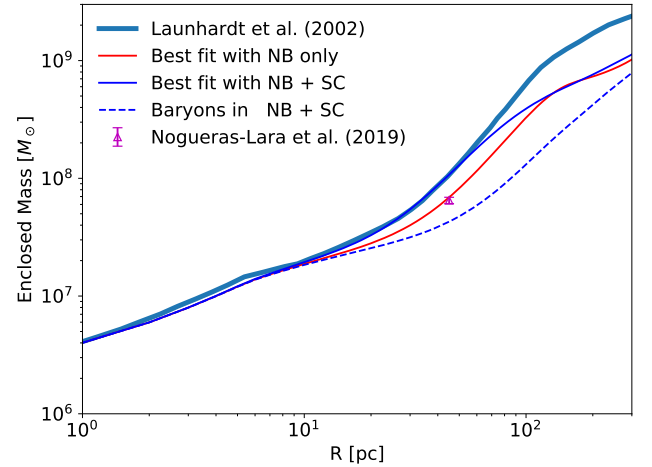


Figure 7. Enclosed mass in spheres of radius R for the inner 300 pc of the Galaxy. The thick blue line is the result from Fig. 14 in Launhardt et al. (2002). The red solid line shows the mass distribution in Fig. 3(d), which is our best-fit model that includes only the nuclear bulge. The blue solid line shows that used in Figs. 4(f) and 5(f), which is one of our best-fit models that contains both the nuclear bulge and the soliton core. The blue dashed line plots the baryonic mass in this model. The purple triangle is the stellar mass ($6.5 \pm 0.4 \times 10^7 M_\odot$) obtained by Noguera-Lara et al. (2019) at 45 pc. Note that this mass is not the enclosed mass inside a $r = 45 \text{ pc}$ sphere, but the total mass inside a $R = 45 \text{ pc}$ and $z = 20 \text{ pc}$ cylinder. We also include a $2.6 \times 10^6 M_\odot$ black hole and a $3.0 \times 10^7 M_\odot$ nuclear stellar cluster in the models to be consistent with Launhardt et al. (2002).

3.5. What does a light and compact soliton core imply?

We use $M_{\text{smax}} = 1.44 \times 10^9 M_\odot$ as the maximum soliton mass inside the Milky Way, which is predicted by the halo-core relation in Schive et al. (2014b) assuming $m_{22} = 1$. However, the accepted models in Figs. 4 and 5 prefer much smaller soliton core mass M_s compared to M_{smax} . In this section we demonstrate that these light and compact soliton cores correspond to a boson mass range of $m_{22} \approx 2 - 7$.

Schive et al. (2014b) presented the relation between self-gravitating soliton core properties ($M_{\text{smax}}, r_{c,0}$) and m_{22} as:

$$\begin{aligned} M_{\text{smax}} &= 1.44 m_{22}^{-1} \times 10^9 M_\odot, \\ r_{c,0} &= 0.16 m_{22}^{-1} \text{ kpc}, \end{aligned} \quad (4)$$

assuming the Milky Way halo mass is $1.5 \times 10^{12} M_\odot$. We use $r_{c,0}$ to denote the core radius of a soliton without compression. Once m_{22} is fixed, M_{smax} and $r_{c,0}$ are determined for a given halo mass. A larger m_{22} corresponds to a less massive and more concentrated soliton core. However, due to the compression by the nuclear bulge, the real core radius r_c should be smaller than the original $r_{c,0}$, as we have shown in §2.1.3. We

therefore define a dimensionless compression parameter $C = r_c/r_{c,0}$ to describe the level of compression. The compressed core radius r_c can be written as:

$$r_c = 231 C \frac{10^9 M_\odot}{M_s} m_{22}^{-2} \text{ pc}, \quad (5)$$

which is independent of the halo virial mass. Substituting $C = r_c/r_{c,0}$ in Eq. 5 recovers the original results in Schive et al. (2014b). Here $C = 1$ corresponds to a self-gravitating soliton core, while for $C < 1$ the soliton core is compressed by baryons. Eqs. 4 and 5 suggest that for a given soliton mass and core radius (M_s, r_c), there is a degeneracy between the boson mass m_{22} and the compression parameter C . In other words, both C and m_{22} can be varied accordingly to give the desired r_c for a certain M_s .

We first show that the compression parameter C in our best-fit models cannot be achieved by the background $\Upsilon = 0.5$ nuclear bulge if m_{22} is around 1. The parameter set (M_s, r_c) of our best-fit models in Figs. 4 and 5, i.e. panels (b, e, f, i, j), can be interpreted as $C = 0.16, 0.04, 0.08, 0.04, 0.02$ with $m_{22} = 1$, as suggested by Eq. 5. We numerically solve the Schrödinger-Poisson equation based on the method in Bar et al. (2019) to self-consistently derive the soliton core radius r_c in the $\Upsilon = 0.5$ nuclear bulge potential. We find r_c should be around 160 pc, 184 pc, and 196 pc for a soliton core with mass of $1/2, 1/4$, and $1/8 M_{\text{smax}}$, assuming $m_{22} = 1$. The corresponding C is therefore 0.50, 0.29, 0.29, 0.15, 0.15 for panels (b, e, f, i, j), about 3–7 times larger than the numbers quoted above. This implies $m_{22} = 1$ cannot produce the preferred soliton cores in Figs. 4 and 5.

On the other hand, a higher boson mass m_{22} naturally produces less massive and more concentrated soliton cores, as both soliton core mass M_s and core radius r_c are inversely proportional to m_{22} . By solving the Schrödinger-Poisson equation, we find $m_{22} = 2.4$ could produce the compressed soliton core with $M_s = 7.2 \times 10^8 M_\odot$ and $r_c = 50$ pc in Fig. 5(b), under the $\Upsilon = 0.5$ nuclear bulge potential we adopt. Similarly, Fig. 5(e) corresponds to $m_{22} = 5.0$, Fig. 5(f) corresponds to $m_{22} = 3.3$, Fig. 5(i) corresponds to $m_{22} = 7.0$, and Fig. 5(j) corresponds to $m_{22} = 4.4$.

Considering all the models highlighted by the red box (i.e. b, e, f, i, and j) in Figs. 4 and 5, we conclude that a boson mass m_{22} in the range of 2–7 is more reasonable in the current configuration of the Galactic potential that contains both the soliton core and the nuclear bulge.

We need to emphasize that our upper limit for m_{22} comes from the assumption that a minimum mass for the soliton core must exist, otherwise the CMZ will not form. However, as shown in §3.2, a nuclear bulge only

model could also form a reasonable CMZ consistent with observed kinematics, as long as we assume the nuclear bulge to be more concentrated than that in Launhardt et al. (2002). Therefore the upper limit we get (i.e. $m_{22} \leq \sim 7$) is only a weak constraint – it could be larger than 7 if the nuclear bulge in reality is more compact in mass compared to the model we adopt in the current paper. On the other hand, the lower limit should be a stronger constraint (i.e. $m_{22} \geq \sim 2$), as we have already assumed a relatively less massive nuclear bulge compared to previous studies.

4. DISCUSSIONS

4.1. The possibility of a higher boson mass

As pointed out above, a m_{22} range of 2–7 is preferred in this work. This boson mass range is marginally higher than the conventional value $m_{22} \approx 1$ (e.g. Schive et al. 2014a), but it is generally consistent with many astrophysical constraints, for example, classical dwarf spheroidal galaxies ($m_{22} = 1 - 2$; Chen et al. 2017), ultra-faint dwarf galaxies ($m_{22} = 3.7 - 5.6$; Calabrese & Spergel 2016), ultra-diffuse galaxy Dragonfly 44 ($m_{22} \approx 3$; Wasserman et al. 2019), stellar streams in the Milky Way ($m_{22} > 1.5$; Amorisco & Loeb 2018), supermassive black holes ($m_{22} > 2.0$ or $m_{22} < 0.63$; Yarnell Davies & Mocz 2019). However, our m_{22} range is still smaller than the results constrained by the rotation curves of low surface brightness galaxies ($m_{22} \geq 10$; Bar et al. 2018, 2019). The larger boson mass also helps alleviate the tension arising from the high- z luminosity function (e.g. Schive et al. 2016; Corasaniti et al. 2017; Schive & Chiueh 2018) and Lyman- α forest (e.g. Iršič et al. 2017; Leong et al. 2019), where either a larger boson mass or an extreme axion model is typically required to produce a sufficient amount of small-scale structure. Self-consistent FDM hydrodynamical simulations will be essential for narrowing down the mass constraints further.

4.2. Central mass profile of the Milky Way

The CMZ size and kinematics constrain the total mass profile in the central ~ 200 pc, but it is still not quite clear whether the central mass is contributed by a compact stellar nuclear bulge, or a less compact nuclear bulge together with a dark soliton core. This mass degeneracy between a nuclear bulge and a soliton core was first discussed in Bar et al. (2018), and a better determination on the mass-to-light ratio of the nuclear bulge (i.e. stellar mass) would be helpful to break this degeneracy. In Fig. 7 we plot the enclosed mass profiles for two of our best-fit models with and without the soliton core. The red solid line in Fig. 7 shows the enclosed mass profile from our nuclear bulge only model (Fig. 3(d)), the central mass in this model are contributed entirely by

baryons. The blue solid line shows the enclosed mass profile from the model that contains both a soliton core and the nuclear bulge (Figs. 4(f) and 5(f)). The mass of the baryonic component (i.e. the nuclear bulge) in this model is plotted with the blue dashed line. We could see that the difference between the baryonic mass of these two models is only about a few $10^7 M_\odot$ at $R \approx 50$ pc. Recently, [Nogueras-Lara et al. \(2019\)](#) obtained the stellar mass in the central 45 pc to be $6.5 \pm 0.4 \times 10^7 M_\odot$ using the *GALACTICNUCLEUS* survey, their results are indicated by the purple triangles with tiny error-bars in this plot. We see that this stellar mass is quite consistent with our nuclear bulge only model without a soliton core. If their mass estimation is accurate, then there is little room left for the FDM soliton core in the Milky Way center. Nevertheless, we still need further observations to provide tighter constraints on the baryon mass profile to better clarify this problem.

4.3. Other dynamical effects of the soliton core

We find that a soliton core with a mass of $\approx 3.6 \times 10^8 M_\odot$ and a nuclear bulge with $\Upsilon = 0.5$ would generate a CMZ that matches the observations relatively well. The total mass of these two components is therefore $\approx 0.7 \times 10^9 M_\odot$. However, the velocity dispersion revealed by *Gaia* and VVV surveys at $|l| \lesssim 10^\circ$ requires a dense center of $\approx 1.5 \times 10^9 M_\odot$ as found by [De Martino et al. \(2018\)](#) and [Portail et al. \(2017\)](#), which is about 2 times larger than the value preferred here. We emphasize that the mass obtained in this paper are constraint mainly by the CMZ region. The CMZ size and kinematics offers no strong constraints on the mass profile outside $R \gtrsim 200$ pc ($|l| \gtrsim 1.5^\circ$). Therefore this discrepancy could be explained by additional mass outside the CMZ radius which could still result a large velocity dispersion. Indeed, the central velocity dispersion of the stars drops inside $R \lesssim 200$ pc ([De Martino et al. 2018](#)), implying a toroidal mass distribution of a less massive center and a more massive periphery.

Interestingly, the soliton core could form such a toroidal shape due to the baryonic potential as reported in [Bar et al. \(2019\)](#). We emphasize that a toroidal soliton core is just one possible solution. More detailed modelling is still needed to predict the exact soliton core properties in the Milky Way.

4.4. Different physical condition of the gas inside CMZ

The gas in the CMZ is multi-phase (e.g. [Langer et al. 2017](#)), but it seems that both the cold and hot gas form a consistent feature in the (l, v) space for which we are trying to match using our isothermal simulations. The isothermal equation of state is a simple assumption, and it forms a slightly smaller CMZ compared to the simulations with a complicated chemistry cooling network,

as shown in [Sormani et al. \(2018b\)](#). The cooling mechanism also helps to break the high density gas in the CMZ into small clumps seen in the NH_3 data, while in our simulation the gas is more smoothly distributed in the CMZ. The cooling time scale for the ISM is much shorter than the dynamical time, thus we expect the kinematics of the CMZ would not be significantly affected by considering the chemical evolution. The mass of the gas in CMZ is around $3.0 \times 10^7 M_\odot$ ([Launhardt et al. 2002](#)), which is also small compared to the mass of the soliton core and the nuclear bulge used in this paper.

In general, including self-gravity and cooling would make the CMZ larger (e.g. [Kim et al. 2012a](#); [Sormani et al. 2018b](#)), while including magnetic field, star formation, and stellar feedback would make it smaller (e.g. [van de Ven & Chang 2009](#); [Kim & Stone 2012](#)). These physics basically influence condition (2) mentioned in §3.2, i.e. where the inflowed gas piles up. Condition (1) is still determined mainly by the gravitational potential. A recent work by [Armillotta et al. \(2019\)](#) studied the star formation in the CMZ with a detailed modelling of gas physics and the stellar evolution. In their models a CMZ of ≈ 200 pc forms, very similar to the isothermal case with the same Galactic potential adopted in [Ridley et al. \(2017\)](#). We therefore regard our isothermal simulations as a first-order approximation to the more complicated simulations. We will explore further the effects of these baryonic physics on the constraints of the soliton core in follow up studies.

4.5. The 3D structure of the CMZ

We have verified that 3D simulations produce very similar gas flow patterns as in the 2D case. Gas cannot go very far above the plane because the deep gravitational potential caused by the soliton core and the nuclear bulge. The edge-on ∞ -shape of the CMZ discovered by [Molinari et al. \(2011\)](#) can also be seen in our 3D simulations. However, the ∞ -shape in the simulations exists only in the first ~ 200 Myr then gradually decays, as also reported in the SPH simulations of [Shin et al. \(2017\)](#). Since it is a transient feature, we prefer not to use it as an indicator to constrain the possible existence of the soliton core. The observed ∞ -shape of the CMZ might be caused by a recent inflow, as suggested in [Sormani & Barnes \(2019\)](#).

5. SUMMARY

We have performed high resolution hydrodynamical simulations of bar-driven gas flows in a realistic Milky Way potential, considering both the effects of a baryonic nuclear bulge and a possible dark soliton core. The observed size and kinematics of the Central Molecular Zone (CMZ) could be reproduced by including a compact cen-

tral mass component, whose mass profile is relatively well-constrained by our models. If a soliton core is not considered, a more compact nuclear bulge than usually assumed could match the observed size and kinematics of the CMZ. Including a moderate soliton core together with a less massive nuclear bulge, also nicely agrees with observations. An effective sound speed of gas around 20 km s^{-1} can help further improve the match. The preferred soliton core could be achieved if the boson mass is larger than the conventional $1.0 \times 10^{-22} \text{ eV}$ by a factor of $2 - 7$. Such a boson mass range is also broadly consistent with many other astrophysical constraints. This mass range can be further narrowed down by the improved determination of the mass-to-light ratio of the nuclear bulge. The 3D ∞ -shape structure of the CMZ probably does not offer a tighter constraint on the soliton core since it is likely a transient feature that occurs only at the beginning of the inflow process. This may imply that the current CMZ may have just experienced a recent inflow, which also helps to explain the low star formation rate in the CMZ caused by a large gas velocity dispersion.

We would like to thank Scott Tremaine for helpful discussions and comments. We thank the anonymous referee for a constructive report, and for helping us solving Schrödinger-Poisson equation under an external potential. We also thank Jonathan Henshaw for sharing the NH_3 data with us. ZL would like to thank Zhang Jiajun for providing comments which have helped to improve the presentation of the paper. H.S. is grateful to Tzihong Chiueh and Tom Broadhurst for stimulating discussions. The research presented here is partially supported by the National Key R&D Program of China under grant no. 2018YFA0404501, by the National Natural Science Foundation of China under grant nos. 11773052, 11333003, 11761131016, and by a China-Chile joint grant from CASSACA. J.S. acknowledges support from an *Newton Advanced Fellowship* awarded by the Royal Society and the Newton Fund. H.S. acknowledges the funding support from the Jade Mountain Young Scholar Award no. NTU-108V0201, MOST of Taiwan under the grant no. 108-2112-M-002-023-MY3, and the NTU Core Consortium project under the grant no. NTU-CC-108L893401. This work made use of the facilities of the Center for High Performance Computing at Shanghai Astronomical Observatory.

REFERENCES

- Amorisco, N. C., & Loeb, A. 2018, arXiv e-prints, arXiv:1808.00464
- Armillotta, L., Krumholz, M. R., Di Teodoro, E. M., & McClure-Griffiths, N. M. 2019, MNRAS, 490, 4401
- Athanassoula, E. 1992, MNRAS, 259, 345
- Baba, J., Saitoh, T. R., & Wada, K. 2010, PASJ, 62, 1413
- Bally, J., Stark, A. A., Wilson, R. W., & Henkel, C. 1988, ApJ, 324, 223
- Bar, N., Blas, D., Blum, K., & Sibiryakov, S. 2018, PhRvD, 98, 083027
- Bar, N., Blum, K., Eby, J., & Sato, R. 2019, PhRvD, 99, 103020
- Bennett, C. L., Larson, D., Weiland, J. L., et al. 2013, ApJS, 208, 20
- Bovy, J., & Rix, H.-W. 2013, ApJ, 779, 115
- Bullock, J. S., & Boylan-Kolchin, M. 2017, ARA&A, 55, 343
- Calabrese, E., & Spergel, D. N. 2016, Monthly Notices of the Royal Astronomical Society, 460, 4397
- Chen, S.-R., Schive, H.-Y., & Chiueh, T. 2017, MNRAS, 468, 1338
- Conroy, C., & Gunn, J. E. 2010, ApJ, 712, 833
- Conroy, C., Gunn, J. E., & White, M. 2009, ApJ, 699, 486
- Corasanti, P. S., Agarwal, S., Marsh, D. J. E., & Das, S. 2017, Phys. Rev. D, 95, 083512
- Dame, T. M., Hartmann, D., & Thaddeus, P. 2001, ApJ, 547, 792
- de Blok, W. J. G. 2010, Advances in Astronomy, 2010, 789293
- De Martino, I., Broadhurst, T., Tye, S. H. H., Chiueh, T., & Schive, H.-Y. 2018, arXiv e-prints, arXiv:1807.08153
- Few, C. G., Dobbs, C., Pettitt, A., & Konstantin, L. 2016, MNRAS, 460, 4382
- Frenk, C. S., & White, S. D. M. 2012, Annalen der Physik, 524, 507
- Fux, R. 1999, A&A, 345, 787
- Gardiner, T. A., & Stone, J. M. 2005, Journal of Computational Physics, 205, 509
- Henshaw, J. D., Longmore, S. N., Kruijssen, J. M. D., et al. 2016, MNRAS, 457, 2675
- Hu, W., Barkana, R., & Gruzinov, A. 2000, PhRvL, 85, 1158
- Hui, L., Ostriker, J. P., Tremaine, S., & Witten, E. 2017, PhRvD, 95, 043541
- Iršič, V., Viel, M., Haehnelt, M. G., Bolton, J. S., & Becker, G. D. 2017, Phys. Rev. Lett., 119, 031302
- Kauffmann, J. 2016, in IAU Symposium, Vol. 315, From Interstellar Clouds to Star-Forming Galaxies: Universal Processes?, ed. P. Jablonka, P. André, & F. van der Tak, 163–166
- Kim, W.-T., Kim, Y., & Kim, J.-G. 2014, ApJ, 789, 68
- Kim, W.-T., Seo, W.-Y., & Kim, Y. 2012a, ApJ, 758, 14
- Kim, W.-T., Seo, W.-Y., Stone, J. M., Yoon, D., & Teuben, P. J. 2012b, ApJ, 747, 60
- Kim, W.-T., & Stone, J. M. 2012, ApJ, 751, 124
- Kruijssen, J. M. D., Dale, J. E., & Longmore, S. N. 2015, MNRAS, 447, 1059
- Kunder, A., Koch, A., Rich, R. M., et al. 2012, AJ, 143, 57
- Langer, W. D., Velusamy, T., Morris, M. R., Goldsmith, P. F., & Pineda, J. L. 2017, A&A, 599, A136
- Launhardt, R., Zylka, R., & Mezger, P. G. 2002, A&A, 384, 112
- Leong, K.-H., Schive, H.-Y., Zhang, U.-H., & Chiueh, T. 2019, MNRAS, 484, 4273
- Leroy, A. K., Walter, F., Bigiel, F., et al. 2009, AJ, 137, 4670
- Li, Z., Gerhard, O., Shen, J., Portail, M., & Wegg, C. 2016, ApJ, 824, 13
- Li, Z., Sellwood, J. A., & Shen, J. 2017, ApJ, 850, 67
- Li, Z., Shen, J., & Kim, W.-T. 2015, ApJ, 806, 150
- Li, Z.-Z., Qian, Y.-Z., Han, J., et al. 2019, arXiv e-prints, arXiv:1912.02086

- Longmore, S. N., Walsh, A. J., Purcell, C. R., et al. 2017, MNRAS, 470, 1462
- Marsh, D. J. E., & Silk, J. 2014, MNRAS, 437, 2652
- Molinari, S., Bally, J., Noriega-Crespo, A., et al. 2011, ApJL, 735, L33
- Navarro, J. F., Frenk, C. S., & White, S. D. M. 1997, ApJ, 490, 493
- Nogueras-Lara, F., Schödel, R., Gallego-Calvente, A. T., et al. 2019, arXiv e-prints, arXiv:1910.06968
- Oñorbe, J., Boylan-Kolchin, M., Bullock, J. S., et al. 2015, MNRAS, 454, 2092
- Portail, M., Gerhard, O., Wegg, C., & Ness, M. 2017, MNRAS, 465, 1621
- Portail, M., Wegg, C., Gerhard, O., & Martinez-Valpuesta, I. 2015, MNRAS, 448, 713
- Posti, L., & Helmi, A. 2019, A&A, 621, A56
- Read, J. I., Walker, M. G., & Steger, P. 2019, MNRAS, 484, 1401
- Regan, M. W., & Teuben, P. 2003, ApJ, 582, 723
- Ridley, M. G. L., Sormani, M. C., Treß, R. G., Magorrian, J., & Klessen, R. S. 2017, MNRAS, 469, 2251
- Rodriguez-Fernandez, N. J., & Combes, F. 2008, A&A, 489, 115
- Sánchez, S. F., Kennicutt, R. C., Gil de Paz, A., et al. 2012, A&A, 538, A8
- Schive, H.-Y., & Chiueh, T. 2018, MNRAS, 473, L36
- Schive, H.-Y., Chiueh, T., & Broadhurst, T. 2014a, Nature Physics, 10, 496
- Schive, H.-Y., Chiueh, T., Broadhurst, T., & Huang, K.-W. 2016, ApJ, 818, 89
- Schive, H.-Y., Liao, M.-H., Woo, T.-P., et al. 2014b, PhRvL, 113, 261302
- Schönrich, R., Aumer, M., & Sale, S. E. 2015, ApJL, 812, L21
- Shin, J., Kim, S. S., Baba, J., et al. 2017, ApJ, 841, 74
- Sormani, M. C., & Barnes, A. T. 2019, MNRAS, 484, 1213
- Sormani, M. C., Binney, J., & Magorrian, J. 2015a, MNRAS, 449, 2421
- . 2015b, MNRAS, 451, 3437
- . 2015c, MNRAS, 454, 1818
- Sormani, M. C., Sobacchi, E., Fragkoudi, F., et al. 2018a, MNRAS, 481, 2
- Sormani, M. C., Sobacchi, E., Shore, S. N., Treß, R. G., & Klessen, R. S. 2017, MNRAS, 471, 2932
- Sormani, M. C., Treß, R. G., Ridley, M., et al. 2018b, MNRAS, 475, 2383
- Stone, J. M., & Gardiner, T. 2009, NewA, 14, 139
- Stone, J. M., Gardiner, T. A., Teuben, P., Hawley, J. F., & Simon, J. B. 2008, ApJS, 178, 137
- van de Ven, G., & Chang, P. 2009, ApJ, 697, 619
- Wada, K., & Koda, J. 2004, MNRAS, 349, 270
- Walter, F., Brinks, E., de Blok, W. J. G., et al. 2008, AJ, 136, 2563
- Wasserman, A., van Dokkum, P., Romanowsky, A. J., et al. 2019, arXiv e-prints, arXiv:1905.10373
- Wegg, C., & Gerhard, O. 2013, MNRAS, 435, 1874
- Weinberg, D. H., Bullock, J. S., Governato, F., Kuzio de Naray, R., & Peter, A. H. G. 2015, Proceedings of the National Academy of Science, 112, 12249
- Yarnell Davies, E., & Mocz, P. 2019, arXiv e-prints, arXiv:1908.04790